Three-Dimensional Shear in Granular Flow

Xiang Cheng,[1] Jeremy B. Lechman,[2] Antonio Fernandez-Barbero,[1,*] Gary S. Grest,[2] Heinrich M. Jaeger,[1]
Greg S. Karczmar,[3] Matthias E. Möbius,[1] and Sidney R. Nagel[1]

[1]*The James Franck Institute and Department of Physics, The University of Chicago, Chicago, Illinois 60637, USA*
[2]*Sandia National Laboratories, Albuquerque, New Mexico 87185, USA*
[3]*Department of Radiology, The University of Chicago, Chicago, Illinois 60637, USA*
(Received 23 July 2005; published 23 January 2006)

The evolution of granular shear flow is investigated as a function of height in a split-bottom Couette cell. Using particle tracking, magnetic-resonance imaging, and large-scale simulations, we find a transition in the nature of the shear as a characteristic height H^* is exceeded. Below H^* there is a central stationary core; above H^* we observe the onset of additional axial shear associated with torsional failure. Radial and axial shear profiles are qualitatively different: the radial extent is wide and increases with height, while the axial width remains narrow and fixed.

Shear bands in dense granular materials are localized regions of large velocity gradients; they are the antithesis of the broad uniform flows seen in slowly sheared Newtonian fluids [1–6]. Until recently it was generally assumed that all granular shear bands were narrow. However, in 2003 Fenistein *et al.* [7] discovered that in modified Couette cells granular shear bands can be made arbitrarily broad. In this geometry, the bottom of a cylindrical container is split at radius $r = R_s$ and shear is produced by rotating both the outer ring and the cylindrical boundary of the container while keeping the central disk ($r < R_s$) stationary. For very shallow packs, the shear band measured at the top surface is narrow and located at $r = R_s$ so that the inner region directly above the central disk is stationary while the remaining part rotates as a solid. As the filling height of the material, H, increases, the shear band increases in radial width and moves toward the cylinder axis. For sufficiently large H, the shear band overlaps the axis at $r = 0$ and one might expect qualitatively new behavior. Indeed, Unger *et al.* [8] predicted that the shape of the boundary between moving and stationary material would undergo a first-order transition as H is increased past a threshold value H^*: the shearing region which for $H < H^*$ is open at the top and intersects the free surface abruptly collapses to a closed cupola completely buried inside the bulk.

Previous experiments focused primarily on the surface flows in shallow containers and left unexplored many questions about the shape and evolution of the shear profiles for large H. Here, we combine magnetic-resonance imaging (MRI) and high-speed video observations with large-scale simulations to explore shear flow both for shallow and tall packs. In addition to monitoring the evolution of the flow profiles in the radial direction, we also examine shear in the vertical direction. Instead of a first-order collapse of the shear zone as proposed by Unger *et al.* [8], we find that above $H^* \simeq 0.6R_s$ the inner core of

immobile material disappears gradually as shear along the central axis of the cylinder sets in.

Our setup is similar to that of Fenistein *et al.* [7], except that we rotate the inner disk instead of the outer ring and cylinder [Fig. 1(b), inset]. In the absence of inertial effects, this makes no difference in the results. For surface observations with high-speed video, we use a cylindrical cell with radius $R_{out} = 72.25$ mm whose bottom is split at $R_s = 55.5$ mm. For the MRI experiments a cell with
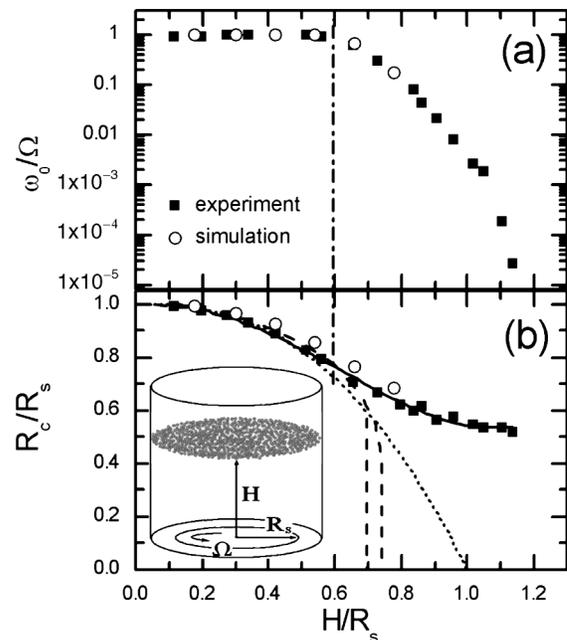

FIG. 1. Surface flow as function of filling height, H. (a) Angular velocity, ω_0 at the cell axis. (b) Center of the shear band, R_c. The solid line is a Gaussian fit to guide the eye; the dotted line is the fitting function of Fenistein *et al.* [7]; the dashed line is the theoretical result [8]. The vertical dash-dotted line indicates $H = 0.6R_s$. Inset: Schematic of split-bottom Couette cell.

$R_{out} = 43.9$ mm and $R_s = 32.5$ mm is used. The inner disk is rotated at angular velocities, Ω, in the shear-rate-independent regime. For the data presented here $\Omega = 1.96$ and 1.01 rad/s for the surface and MRI experiments, respectively. We fill the cell with granular material to a total height $h = H$, measured from the cell bottom. A layer of grains glued to the cell walls and bottom assures controlled friction at the boundaries. For the surface flow measurements we used spherical mustard seeds ($d = 1.9$ mm) and tracked their motion with high-speed video at frame rates ranging from 250 to 0.027 s^{-1}. To follow the motion of particles inside the pack using MRI, we use a mixture of poppy and rajagara seeds. Rajagara seeds are more spherical than poppy seeds [Fig. 2(b), inset] but have nearly the same average diameter ($d = 0.85$ mm) and the same density ($\rho = 1.1$ g/cm^3). Poppy seeds contain more oil than rajagara seeds, providing a clear contrast in MRI signal which allows for particle tracking [Fig. 2(a) inset].

The simulations are carried out with a discrete element method in which grains interact only upon contact through assumed point forces in normal and tangential directions,
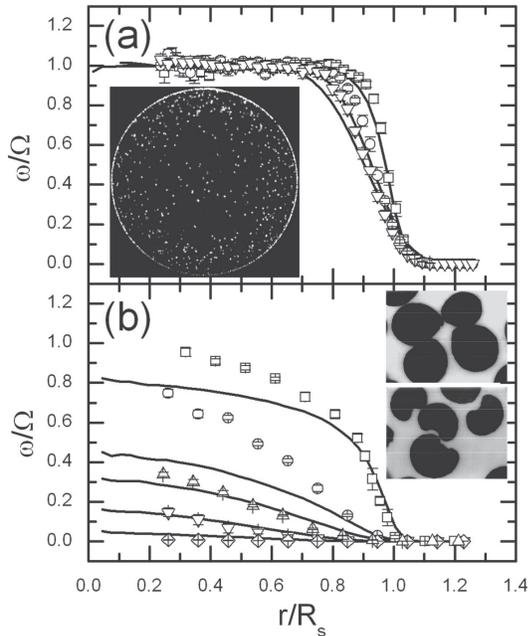

FIG. 2. Angular velocity profiles $\omega(r)$ at different vertical positions h for (a) $H = 0.4R_s$ and (b) $H = 0.88R_s$. Symbols for MRI experiments: (a) $h = 0.21H$ ($\square$), $h = 0.43H$ ($\bigcirc$), and $h = 0.65H$ ($\triangledown$); (b) $h = 0.10H$ ($\square$), $h = 0.21H$ ($\bigcirc$), $h = 0.31H$ ($\triangle$), $h = 0.42H$ ($\triangledown$), and $h = 0.73H$ ($\diamondsuit$). Lines for simulations: (a) (from right to left) $h = 0.19H$, $h = 0.50H$, and $h = 0.85H$; (b) (from top to bottom) $h = 0.11H$, $h = 0.23H$, $h = 0.30H$, $h = 0.43H$, and $h = 0.70H$. Inset of (a): MRI image for one layer inside the bulk. Bright spots are poppy seeds, while dark background are rajagara seeds; poppy seeds glued to the wall of the cell show up as a bright circle. Inset of (b): Optical micrographs of rajagara (top) and poppy seeds (bottom).

and elastic tangential displacements are truncated as necessary to satisfy the Coulomb criteria at the contact. Details of the specific implementation can be found elsewhere [9]. We use monodisperse Hertzian spheres with a layer of frozen particles at the bottom. The relevant parameters describing the material properties of the spheres are the normal stiffness $k_n = 2 \times 10^5$ mg/d, the tangential stiffness $k_t = 2/7k_n$, the normal and the tangential viscous damping coefficients $\gamma_n = 50\sqrt{g/d}$, and $\gamma_t = 0$, and the particle and wall coefficients of friction $\mu = 0.5$, where d and m are the diameter and mass of spheres and g is the gravity acceleration. We have checked that changing the coefficients of friction does not qualitatively change the observed behavior. The cell dimensions used for the simulation match those used for the surface measurement experiments. We choose $\Omega = 0.014\sqrt{d/g} \simeq 1.39$ rad/s.

Evidence for a change in flow behavior with increasing filling height, H, can already be found by tracking particle motion at the free top surface (Fig. 1). The angular velocity at the center of the cell, $\omega_0 = \omega(r = 0, h = H)$, is independent of H for shallow packs but begins to decrease beyond $H^* \simeq 0.6R_s$. At a similar height, Fenistein *et al.* found that the radial shear profile at the surface begins to deviate from the universal error-function shape describing the profile for shallow packs [7]. Dramatic deviations are also seen in the evolution of the center position of the shear band, $R_c(H)$, with filling height [Fig. 1(b)]. Our results for R_c, defined as the radial position where the shear rate has its maximum, are consistent with previous experiments [7] as well as with models [8] in the shallow pack regime. However, while ω_0 decreases for $H > H^*$, the shear zone does not disappear at the surface as predicted by the theory (dashed line). Instead, in both experiments and simulations R_c asymptotically approaches a nonzero value.

These results imply that, beyond H^*, velocity gradients must also exist in the vertical, axial direction near the center of the cell. Our MRI experiments and simulations explore this shear flow inside the bulk. We prepare our MRI samples by mixing 5% (by volume) poppy seeds (MRI positive seeds) uniformly with rajagara seeds [Fig. 2(a), inset]. Images before rotation and after an interval of rotation are taken. By performing a cross correlation of the two images as a function of radius, we obtain velocity profiles $\omega(r)$ as a function of h (Fig. 2). This method enables us to measure velocities with several orders of magnitude difference (for details, see [10]). For both experiments and simulations, care was taken to assure that the systems are in the steady state by rotating long enough before any measurements were performed. As an additional check we made sure that stopping and restarting the system did not change the velocity profile, which is consistent with the previous study [11].

For $H < H^*$, MRI and simulations show an inner core at the center of the pack which rotates as a solid along with the rotating bottom. We plot the profiles $\omega(r)$ in Fig. 2(a).
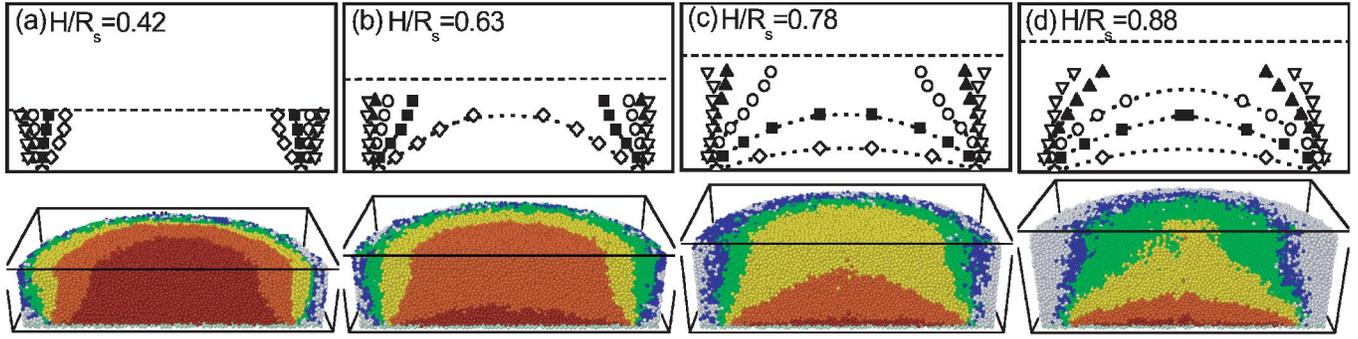
FIG. 3 (color).   Contours of constant angular velocity, ω/Ω, for different filling height H. Upper panels: MRI experiments: $\omega/\Omega =$ 0.84 ($\diamond$), 0.24 ($\blacksquare$), 2.4×10^{-2} ($\bigcirc$), 2.4×10^{-3} ($\blacktriangle$), and 2.4×10^{-4} ($\triangledown$). Dashed lines indicate H and dotted lines are guides to the eye. Lower panels: simulations. Color is used to identify velocity ranges: dark red, $\omega/\Omega \in [0.84, 1]$; orange, $[0.24, 0.84]$; yellow, $[2.4 \times 10^{-2}, 0.24]$; green, $[2.4 \times 10^{-3}, 2.4 \times 10^{-2}]$; blue, $[2.4 \times 10^{-4}, 2.4 \times 10^{-3}]$; white, $[0, 2.4 \times 10^{-4}]$.

There is no slip between different layers near the center of the cell, and the profiles are fit well by an error function. However, when we increase H above H^*, axial slip occurs in both MRI experiments and simulations: the bottom layer rotates at the same rate as the bottom disk, while the layer near the surface hardly rotates at all [Fig. 2(b)] [12]. Thus the decrease in surface flow velocity for $H > H^*$ is caused by shear between horizontal layers inside the bulk. For $H < H^*$, an inner core exists at the center of the cell which rotates with the inner disk with $\frac{\partial \omega(r,h)}{\partial h}|_{r=0} = 0$; while for $H > H^*$, $\frac{\partial \omega(r,h)}{\partial h}|_{r=0} \neq 0$.

To visualize the resulting shear profiles, we plot cross sections of the system with contours of constant angular velocity (Fig. 3). For H well above H^*, the high-velocity contours close into dome shapes [Fig. 3(d)], which gradu-

ally open as H decreases. The contours for smaller velocities open up earlier and eventually touch the surface [Figs. 3(b) and 3(c)]. When $H < H^*$, all velocity contours touch the surface as a solid inner core forms for $r < R_s$ [Fig. 3(a)]. The lower panel shows the corresponding simulation results in a color gradient. One can see how the motion at different h correlates with the motion of the bottom disk.

Having access to the full shear profiles allows us to address the question of whether the same length scale describes the shear in axial and radial directions. Insets (a) and (b) of Fig. 4 show $\omega(h)$ measured along the axis of the cell ($r = 0$) for different heights H. We note that the axial velocity decays in an exponential fashion before the data plateau at a level that extends to the surface. All MRI and simulation data can be fit consistently to a Gaussian form, $\omega(h)/\Omega = a + (1 - a)\exp[-h^2/(2\sigma^2)]$, where a is an H-dependent offset indicating the angular
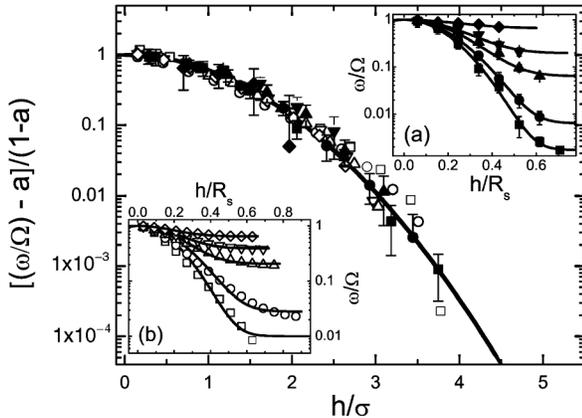

FIG. 4.   Scaled angular velocity $[(\omega/\Omega) - a]/(1 - a)$ for different heights h/σ. Insets show the corresponding unscaled data from (a) MRI and (b) simulations. The main panel uses the same symbols as the insets. The solid line is a Gaussian $\exp[-h^2/(2\sigma^2)]$ with $\sigma = 0.18 R_s$. Inset (a): $H = 0.97 R_s$ ($\blacksquare$), $H = 0.88 R_s$ ($\bullet$), $H = 0.78 R_s$ ($\blacktriangle$), $H = 0.74 R_s$ ($\blacktriangledown$), and $H = 0.63 R_s$ ($\blacklozenge$). Inset (b): $H = 1.02 R_s$ ($\square$), $H = 0.90 R_s$ ($\bigcirc$), $H = 0.78 R_s$ ($\triangle$), $H = 0.72 R_s$ ($\triangledown$), and $H = 0.66 R_s$ ($\diamond$). Solid lines are Gaussian fits introduced in the text.
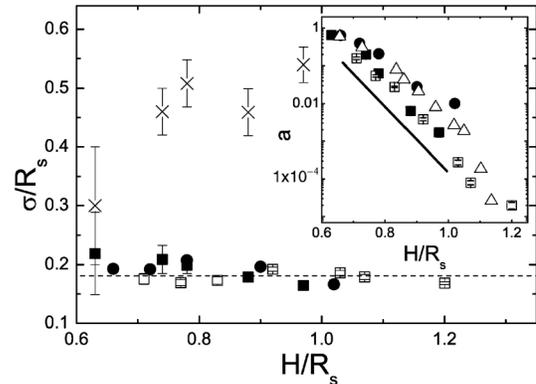

FIG. 5.   Width of the shear profiles, σ, for different filling heights H. Data show σ along both the axial direction in the bulk ($\blacksquare$ and $\square$ from MRI experiments using different methods) [14]; $\bullet$ from simulations) and the radial direction in the surface layer ($\times$). The dashed line is $\sigma = 0.18 R_s$. Inset: offset a vs H from MRI ($\blacksquare$, $\square$) and simulations ($\bullet$). Surface data from Fig. 1 are shown for comparison ($\triangle$). The solid line indicates exponential behavior.

velocity at the top surface and σ is the axial shear-band width. The main panel in Fig. 4 demonstrates the consistency of fitting a Gaussian to the axial shear profile, collapsing data from MRI measurements and simulations. Near H^*, the offset, a, approaches unity in an exponential manner (Fig. 5, inset). Although all data show the same exponential behavior, the offsets from simulations and surface measurement with monodisperse spherical grains are larger than those from the MRI experiments with poppy and rajagara seeds [12]. Extrapolating each set of data to $\omega/\Omega = 1$ suggests that the onset of axial shear begins at $H^* = 0.60 \pm 0.02R_s$.

The data in Fig. 5, together with those from Fig. 1(a), demonstrate that the transition in shearing behavior at H^* occurs in a continuous manner. This differs from the model by Unger *et al.* [8], which predicts a first-order transition at $H^* = 0.7R_s$. While the Unger model, based on the idea of minimum dissipation of energy, includes the essential elements for the transition in the shape of the shear band, a key aspect not considered is the axial slip below H^*. The necessity for such slip emerges from considering the torque balance in shallow packs. When the torque on the surface of the inner core exceeds the frictional strength at the bottom, slip will occur. The total torque on the surface of the inner core and the torsional strength of the contact between the bottom of the cell and the granular material above it can be calculated if the shape of the inner core $h_{core}(r)$ is known. Using the approximate $h_{core}(r)$ given in [8], it can be shown that this already occurs when $H > 0.5R_s$. Thus, already within the Unger model a torsional failure mode near the bottom should preempt any first-order transition within the bulk. Our data demonstrate that this torsional failure is associated with a well-defined axial shear band at $r = 0$ that exhibits a Gaussian profile.

Gaussian shear profiles have been observed in previous studies using traditional Couette cells [5]. However, in the present geometry we find such a profile along the axial direction and an approximate error-function profile along the radial direction. The width of this axial shear zone appears to be independent of H, with an average value $\sigma = 0.18R_s$, implying $\sigma/d = 6.9$ for the experiment and 5.4 for the simulation (Fig. 5). This is in contrast to the width of the radial shear profile (Fig. 5), which strongly depends on H and approaches 0 as $H \rightarrow 0$ [7].

The ubiquitous presence of shear bands is one of the crucial differences between granular materials and ordinary fluids. Understanding what gives rise to the shear profiles is one of the outstanding puzzles in granular dynamics. The modified Couette geometry produces two distinct forms of shear: a radial component whose width grows with height as shown by Fenistein *et al.* [7], and an axial component with a small constant width that appears only when the filling height exceeds a threshold. The different character of the shear bands in the radial and axial directions shows that boundary conditions are essen-tial for determining shear localization. Because the onset of axial shear in this geometry is continuous and controlled simply by the height of the pack, these studies have allowed for detailed observation of how shear can be initiated in the bulk. Very recent surface measurement of the central core procession [13] also corroborates our three-dimensional results.

*Permanent address: Complex Fluids Physics Group, Department of Applied Physics, University of Almeria, Almeria 04120, Spain.
[1] J. Duran, *Sands, Powders, and Grains* (Springer, New York, 2000).
[2] L. Bocquet *et al.*, Phys. Rev. E **65**, 011307 (2002).
[3] R. P. Behringer *et al.*, Physica (Amsterdam) **133D**, 1 (1999).
[4] C. T. Veje, D. W. Howell, and R. P. Behringer, Phys. Rev. E **59**, 739 (1999).
[5] D. M. Mueth *et al.*, Nature (London) **406**, 385 (2000).
[6] M. Toiya, J. Stambaugh, and W. Losert, Phys. Rev. Lett. **93**, 088001 (2004).
[7] D. Fenistein and M. van Hecke, Nature (London) **425**, 256 (2003); D. Fenistein, J. W. van de Meent, and M. van Hecke, Phys. Rev. Lett. **92**, 094301 (2004).
[8] T. Unger *et al.*, Phys. Rev. Lett. **92**, 214301 (2004).
[9] L. E. Silbert *et al.*, Phys. Rev. E **64**, 051302 (2001); L. E. Silbert, J. S. Landry, and G. S. Grest, Phys. Fluids **15**, 1 (2003).
[10] X. Cheng *et al.* (to be published).
[11] B. Utter and R. P. Behringer, Eur. Phys. J. E **14**, 373 (2004).
[12] We believe that the quantitative difference between MRI experiments and simulations is due to the different cell geometry and particle shape used in the two situations. However, they all show the same trend.
[13] D. Fenistein, J. W. van de Meent, and M. van Hecke, cont-mat/0507442.
[14] Solid squares are measured with the method introduced in the text. Open squares are obtained by placing a thin cross of poppy seeds at the center of the cell and measuring its distortion after rotation, similar to [7]. For a detailed discussion of the experimental methods, see [10].